

Article

Intake Valve Profile Optimization for a Piston-Type Expander Based on Load

Yan Shi ¹, Qihui Yu ^{2,3,*}, Guoxin Sun ² and Xiaodong Li ²¹ School of Automation Science and Electrical Engineering, Beihang University, Beijing 100191, China² Department of Mechanical Engineering, Inner Mongolia University of Science & Technology, Baotou 014010, China³ Pneumatic and Thermodynamic Energy Storage and Supply, Beijing Key Laboratory, Beijing 100191, China

* Correspondence: yuqihui@imust.edu.cn; Tel.: +86-131-9069-8276

Abstract: Intake valve parameters significantly affect the performance of the piston-type expander (PTE). To improve compressed energy utilization efficiency, intake valve parameters need to be regulated according to load. In this paper, an electro-pneumatic variable valve actuation (EPVVA) system was proposed for independent control distributing valve parameters. The trajectory planning for the intake valve was proposed to obtain good mechanical properties. Then, the intake valve duration angle was optimized, and the optimum intake valve lift curves were obtained at different rotational speeds. Results show that the energy efficiency decreased with the intake valve duration angle increasing. The output power ascended sharply with increasing intake valve duration angle, but the amplitude of power growth decreased. The output power had a maximum value at a specific intake valve duration angle. The gray relation analysis (GRA) method was applied to obtain the optimum intake duration angle based on output power and energy efficiency. Finally, the optimum intake valve trajectories were presented under different rotational speeds. Results are helpful for the future control of the piston-type expander.

Keywords: variable valve system; electro-pneumatic driving; trajectory planning; intake valve duration angle



Citation: Shi, Y.; Yu, Q.; Sun, G.; Li, X. Intake Valve Profile Optimization for a Piston-Type Expander Based on Load. *Processes* **2023**, *11*, 843. <https://doi.org/10.3390/pr11030843>

Academic Editors: Rosenberg J. Romero and Jesús Cerezo Román

Received: 10 February 2023

Revised: 8 March 2023

Accepted: 9 March 2023

Published: 11 March 2023



Copyright: © 2023 by the authors. Licensee MDPI, Basel, Switzerland. This article is an open access article distributed under the terms and conditions of the Creative Commons Attribution (CC BY) license (<https://creativecommons.org/licenses/by/4.0/>).

1. Introduction

In recent years, energy conservation and carbon emission reduction, crucial global concerns, have drawn considerable attention. Many countries present carbon peak and carbon-neutral policies and put them into practice. As the world's largest developing country globally, China has committed to being carbon peak by 2030 and carbon neutral by 2060 [1]. All the policies show that renewable energy will develop rapidly in the next few years. Nevertheless, renewable energy such as wind and solar power is characterized by intermittency and volatility, causing severe negative impacts on the power grid [2]. The energy storage system (ESS) can effectively cope with this challenging issue due to its flexible charging and discharging capabilities [3].

Compressed air energy storage (CAES) is a concept for thermo-mechanical energy storage with the potential to offer low-cost, large-scale, and fossil-fuel-free operations [4]. With the development of CAES, small-scale systems of CAES are also explored in both academic studies and industrial projects [5–7]. In a CAES system, the expander is a critical component that decides the power output and the overall energy conversion efficiency. The selection of expanders highly depends on both the system operations and the discharge power capacity of the energy storage system [8]. Generally, two main types of expanders can be selected in the market: the positive displacement (volume) type, such as piston-type expanders (PTE), screw and scroll expanders, and the dynamic (velocity) types, such as radial and axial turbines. The PTEs are suitable for scaled-down CAES systems owing to the low flow rate, high-pressure ratio, and low rotational speed [9,10]. The PTE has been

used in marine and stationary power plants and attempts to apply it in the automotive field [11].

PTE as a compressed air engine has been investigated. Mathematical models of compressed air engines were established. The operational characteristics of the engine under both single-stage and two-stage expansion were analyzed by some researchers [12,13]. Liu et al. used a multi-objective optimization method to obtain maximum cycle efficiency under the engine intake pressure ratio at 32 [14]. A virtual prototype with a newly developed valve system was designed to study the compressed air engine's dynamic performance and the optimized valve-controlling strategies [15]. These applications and studies on PTEs have demonstrated the technical viability of this type of expander to be used in the CAES system. However, due to the uncertainty of renewable energy characteristics and load requirements in the CAES system, the expander often works under off-design conditions. The off-design conditions affect the energy efficiency of the expander significantly. Therefore, the PTE usually runs under off-design conditions, which is difficult to run efficiently in a wide range [16].

Based on previous studies, the opening and closing of the inlet and exhaust valves significantly affect the performance of the PTE. However, adjusting the opening and closing of the inlet and exhaust valve is challenging to meet load demand by a cam mechanism. To meet the load demand, Yu et al. proposed a pneumatic circuit that consists of a regulator, air-operated regulator, electronic pressure control unit, and pressure sensor to obtain the requirement load [17] in high pressure and significant flow conditions. However, a large quantity of energy is lost in the throttling process. It is necessary to find a new approach to solve the above problem.

The PTE often works in high-pressure and extensive flow conditions to improve the output power, making airflow regulation difficult. Few variable valve actuation (VVA) technologies for PTE were investigated. In fact, fast-switching pneumatic solenoids can be applied in some high-precision control fields. For example, Shi et al. proposed a pneumatic vibration isolation system based on fast-switching pneumatic solenoids and used pressure difference to improve the system control precision [18,19]. This study aims to provide an electro-pneumatic variable valve actuation system for PTE, and the intake valve duration angle is optimized to obtain high energy efficiency and output torque. In the VVA system, double-acting pneumatic actuators govern the forward and backward motions of the engine valves. Fast-switching pneumatic solenoids control the pressurized air through the actuator. The desired intake and exhaust valve motion profiles are achieved by energizing and de-energizing the solenoids.

The rest of the paper is organized as follows: the system structure, working principle, mathematical model, and trajectory planning are described in detail in Section 1. Simulation and optimization are carried out in Section 2. Section 3 is devoted to the summary and conclusions.

2. Methodology

2.1. EPVVA System of Piston Expander Configuration

The schematic diagram of the EPVVA system of the piston expander is illustrated in Figure 1. The major components include the intake valve actuator, exhaust valve actuator, intake valve, exhaust valve, accumulator, regulator, connectors, preload spring, engine head, piston, link, and crank. The engine intake valve (IEV) and exhaust valve (EEV) are connected to double-acting pneumatic actuators using connectors. The double-acting pneumatic actuator has upper and lower chambers. In this paper, the upper and lower chambers of the intake valve actuator are renamed the a and b chambers. The exhaust valve actuator's upper and lower chambers are called the c and d chambers.

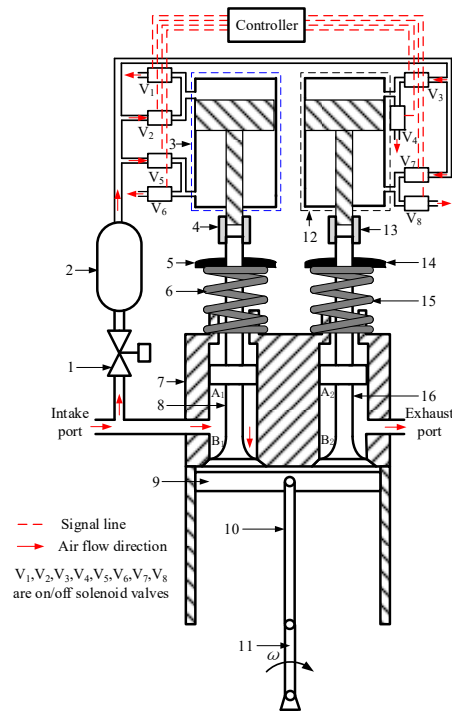


Figure 1. Schematic diagram of EPVVA system. 1 Regulator; 2 Accumulator; 3 Intake valve actuator; 4 13 Connectors; 5, 14 Valve tablet; 6, 15 Preload spring; 7 Engine head; 8 Intake valve; 9 Piston; 10 Link; 11 Crank; 12 Exhaust valve actuators; 16 Exhaust valves.

Pressurized airflow into the actuator is controlled by the solenoids $V_1, V_2, V_3, V_4, V_5, V_6, V_7,$ and V_8 . They are commercially available high-frequency solenoid valves, in which the solenoid’s plunger directly controls the fluid flow. V_1 and V_2 are connected to chamber a, and V_5 and V_6 are connected to chamber b. Each solenoid valve is connected in pairs to achieve the desired mass flow rate controlled according to the crankshaft angle to accomplish the expander intake, expansion, and exhaust processes shown in Figure 2. The working process can be described as follows:

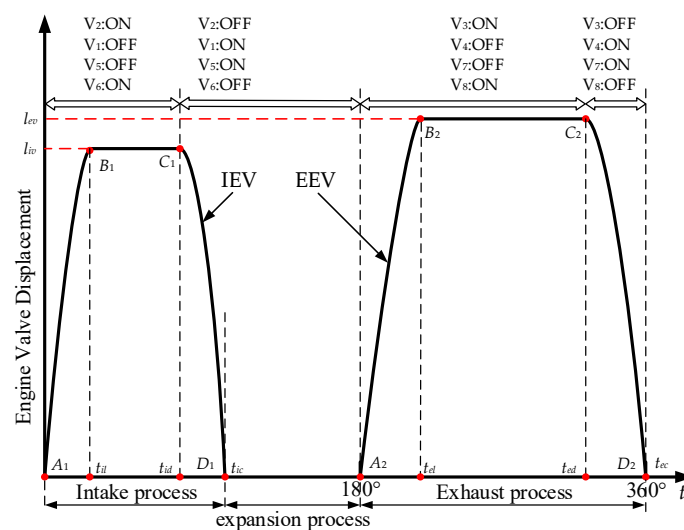


Figure 2. The status of the fast-switching valves at engine operating intervals.

Intake process: when the crankshaft’s angle is equal to 0 degrees, the V_2 solenoid coil is energized, the V_1 solenoid coil is de-energized, the V_5 solenoid coil is de-energized, and the V_6 solenoid coil is energized. The pressurized air from the accumulator flows into

chamber a. The air inside chamber b flows out, and the pressurized air pushes the intake actuator piston connected with the intake valve down to open the IEV. Meanwhile, the pressurized air from the supply-side flows into the expander cylinder through the intake port and pushes the expander piston downward. After the crankshaft's angle reaches point C_1 , the V_2 solenoid coil is de-energized, the V_1 solenoid coil is energized, the V_5 solenoid coil is energized, and the V_6 solenoid coil is de-energized. The pressurized air from the accumulator flows into chamber b, and the residual air inside chamber a flows out until the IEV closes.

Expansion process: the V_2 solenoid coil is de-energized, the V_1 solenoid coil is energized, the V_5 solenoid coil is energized, the V_6 solenoid coil is de-energized, and the IEV is closed. The pressurized air entering the expander cylinder expands and pushes the piston downward to the bottom dead center (BDC).

Exhaust process: when the expander piston reaches BDC, the V_3 solenoid coil is energized, the V_4 solenoid coil is de-energized, the V_7 solenoid coil is de-energized, and the V_8 solenoid coil is energized. The pressurized air from the constant pressure air tank flows into chamber c and pushes the exhaust actuator piston to the exhaust valve to open the EEV. The residual air inside the expander cylinder flows out through the EEV. After the crankshaft's angle reaches point C_2 , the V_3 solenoid coil is de-energized, the V_4 solenoid coil is energized, the V_7 solenoid coil is energized, the V_8 solenoid coil is de-energized. The pressurized air from the accumulator flows into chamber d, and the residual air inside chamber c flows out until the EEV closes.

2.2. Expander Mathematical Model

The following assumptions were made:

- (1) The working air of the system follows all ideal gas laws.
- (2) There is no leakage in the working process, and the area of the piston rod end is too small to be considered.
- (3) Supply temperature is equal to atmospheric temperature.
- (4) The flow of air moving into and out of the cylinder is a stable one-dimensional flow.

Because there is no leakage in the working process, the charge and discharge of air does not simultaneously happen. The heat transfer can be neglected during the active process, owing to the high operation speed. The following equation can illustrate the energy equation for the expander:

$$c_v m_{cy} \frac{dT_{cy}}{dt} = (c_p T_{atm} - c_v T_{cy}) G_{ic} - RT_{cy} G_{oc} - p_{cy} \frac{dV_{cy}}{dt} \quad (1)$$

where c_v is the specific heat at constant volume, c_p is the specific heat at constant pressure, m_{cy} is the air mass of cylinder, T_{cy} is the air temperature of cylinder, T_{atm} is the atmosphere temperature, G_{ic} is the intake air mass flow, G_{oc} is the exhaust air mass flow, p_{cy} is the air pressure of cylinder, V_{cy} is the air volume of the cylinder, and R is the gas constant.

The intake air mass flow G_{ic} and the exhaust air mass flow G_{oc} can be calculated by:

$$G_i = \begin{cases} A_{ei} p_H \sqrt{\frac{k}{RT_H} \left(\frac{2}{k+1}\right)^{\frac{k+1}{k-1}}} & p_L/p_H \leq 0.528 \\ A_{ei} p_H \sqrt{\frac{2k}{(k-1)RT_H} \left[(p_L/p_H)^{2/k} - (p_L/p_H)^{k+1/k} \right]^{k+1/k}} & p_L/p_H > 0.528 \end{cases} \quad (2)$$

where the subscripts H and L denote the upstream and downstream compressed air. The subscript i indicates the intake air or exhaust air, A_e is the effective area, and k is the adiabatic exponent, equal to 1.4.

The valve area of the frustum-shaped site is calculated by:

$$A_{ei} = N_v \pi l_v \cos a (D_s + l_v \cos a \sin a) \quad (3)$$

where a is the valve face angle, N_v is the number of the intake valve and exhaust valve, D_s is the diameter of the valve small head, and l_v is the valve displacement.

Using the ideal gas law, the engine cylinder pressure is determined by:

$$p_{cy} = \frac{m_{cy}RT_{cy}}{V_{cy}} \quad (4)$$

$$V_{cy} = A_{cy}(x + x_0) \quad (5)$$

where A_{cy} , x , and x_0 are the area of the piston, the piston displacement, and cylinder clearance, respectively.

In the above equation, x is the piston displacement, which is calculated by:

$$x = r_{cs} + L_{rod} - r_{cs} \cos(\theta_{cs}) - \sqrt{L_{rod}^2 - r_{cs}^2 \sin^2(\theta_{cs})} \quad (6)$$

where r_{cs} , L_{rod} , and θ_{cs} are the crank radius (half stroke), piston rod length, and crank angle, respectively.

2.3. Evaluation Indicator

If the friction torque is neglected, in a steady state, the output torque can be expressed as:

$$T_{or} = T_i - T_r \quad (7)$$

where T_i is the indicated torque, and T_r is the reciprocating torque.

The relationship between the in-cylinder pressure p_{cy} and the indicated torque T_i can be expressed as:

$$T_i = (p_{cy} - p_{atm}) A_{cy} r_{cs} G(\theta_{cs}) \quad (8)$$

where

$$G(\theta_{cs}) = \frac{\sin(\theta_{cs} + \beta)}{\cos \beta} \quad (9)$$

$$\beta = \sin^{-1} \frac{r_{cs} \sin \theta_{cs}}{L_{rod}} \quad (10)$$

The reciprocating torque is given by:

$$T_r = Mr_{cs}^2 G(\theta_{cs}) G_1(\theta_{cs}) \dot{\theta}_{cs}^2 \quad (11)$$

where

$$G_1(\theta_{cs}) = \cos(\theta_{cs}) + \frac{\lambda \sin(\theta_{cs}) \cos(\theta_{cs})}{(1 - \lambda^2 \sin^2(\theta_{cs}))^{3/2}} - \frac{\lambda \sin^2(\theta_{cs})}{(1 - \lambda^2 \sin^2(\theta_{cs}))^{1/2}} \quad (12)$$

$$\lambda = \frac{r_{cs}}{L_{rod}} \quad (13)$$

where M is the piston, rings, pin, and small end connecting rod mass.

The output power of the piston expander is expressed as follows:

$$P = \frac{\int T_i/t \times n}{9550} \quad (14)$$

where t is time, and n is the speed of the crankshaft (rpm).

Energy utilization efficiency can be expressed as:

$$\eta = \frac{P}{E_{air}} \times 100\% \quad (15)$$

where E_{air} is the air power which can be calculated.

$$E_{air} = G_{ic}RT_{ic} \ln(p_{ic}/p_0) \quad (16)$$

where T_{ic} is the temperature of the supply air. p_{ic} is the pressure of the supply air.

2.4. Trajectory Planning for Engine Valve

A typical valve position and the corresponding valve event performance parameters are shown in Figure 2. Here, l_{iv} is the IEV maximum lift, l_{ev} is the EEV maximum lift, t_{il} is the intake valve up to the maximum lift's corresponding time, t_{id} is the intake valve beginning to the close's corresponding time, and t_{ic} is the intake valve's fully closed corresponding time. Similarly, t_{el} , t_{ed} , and t_{ec} are the exhaust valve's up to maximum lift corresponding time, the exhaust valve's beginning to close corresponding time, and the exhaust valve's fully closing corresponding time.

To minimize energy loss during the valve opening and closing process, t_{il} , $t_{ic} - t_{id}$, $t_{ed} - t_{el}$, and $t_{ec} - t_{ed}$ should reduce as much as possible. The valve velocity should be low when approaching the closing position to avoid the mechanical components' noise, wear, and tear. The typical third-order trajectory planning for the point–point motion is shown in Figure 3, where T_0 and l_{max} represent the movement time from closing to opening and the lift of the engine valve, respectively. The movement distance l can be given as:

$$l = a + bt + ct^2 + dt^3 \tag{17}$$

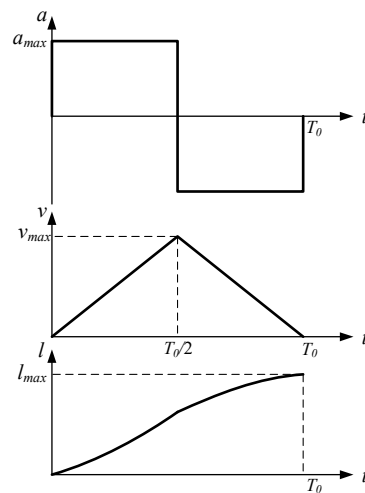


Figure 3. Third-order target trajectory planning.

According to boundary conditions, when $t = 0, l = 0$; when $t = 0, v = 0$; when $t = T_0, v = 0$; when $t = T_0, l = l_{max}$. Based on the above analysis, the date of the trajectory planning is calculated by digital integration, as shown in Equation (18).

$$\begin{cases} a = 0 \\ b = 0 \\ b \cdot T_0 + c \cdot T_0^2 + d \cdot T_0^3 = l_{max} \\ b + 2c \cdot T_0 + 3d \cdot T_0^2 = 0 \end{cases} \tag{18}$$

$A, b, c,$ and d can be calculated by Equation (25).

$$\begin{cases} a = 0 \\ b = 0 \\ c = 3l_{max}/T_0^2 \\ d = -2l_{max}/T_0^3 \end{cases} \tag{19}$$

The opening profile of the valve can be described as:

$$l = 3l_{max}/T_0^2 t^2 - 2l_{max}/T_0^3 t^3 \tag{20}$$

The closing profile of the valve can be obtained by using the same method. Based on the above analysis, the lift curves of IEV and EEV can be described by:

$$l_{iv} = \begin{cases} l_{iv}(t) & t_{up} \leq t < t_{il} \\ l_{imax} & t_{il} \leq t < t_{id} \\ l_{iv}(t_{ic} - t) & t_{id} \leq t < t_{ic} \end{cases} \quad (21)$$

$$l_{ev} = \begin{cases} l_{ev}(t) & t_{down} \leq t < t_{el} \\ l_{emax} & t_{el} \leq t < t_{ed} \\ l_{ev}(t_{ec} - t) & t_{ed} \leq t < t_{ec} \end{cases} \quad (22)$$

$$t_{id} = t_{il} + \theta_{id}/6 \times n \quad (23)$$

where t_{up} is the corresponding time when the piston reaches to top dead center, and t_{down} is the corresponding time when the piston comes to down dead center, θ_{id} is the intake duration angle, n is the rotation speed of the engine, l_{imax} is the maximum lift of intake valve, l_{emax} is the maximum lift of exhaust valve. Additionally, $t_{il} - t_{up}$, $t_{ic} - t_{id}$, $t_{el} - t_{down}$, and $t_{ec} - t_{ed}$ are equal to T_0 .

3. Result and Discussion

3.1. Valve Open and Close Time

As mentioned before, the fast-switching valves are responsible for opening and closing the flow connections between the pneumatic cylinder and the constant pressure tank. The response time and flow rate of the fast-switching valve will influence the pressure of the pneumatic cylinder and then affect the engine valve's kinematic character. The fast switching valve should have a high frequency, high-speed response, and high flow rate to obtain a fast response to the engine valve low rate. Two kinds of fast switching valves can be selected in this work; one is the two 2/2-ways fast switching valve with series number MHJ10-S-2,5-QS-6-HF produced by FESTO company, and the other is the two 2/2-ways fast switching valve of series number SX12-JJ produced by the company SMC. The specifications of the two kinds of switching valves are shown in Table 1.

Table 1. Specification of high-speed on–off valve.

Company	Effective Range (bar)	Response Time of Power on (ms)	Response Time of Power off (ms)	C (dm ³ /(s/bar))	b
FESTO	0.5–6	1.3	0.6	0.66	0.36
SMC	1.5–7	0.6	0.75	0.7	0.21

In Table 1, C is the sonic conductance, and b is the critical pressure ratio. According to the response time and flow rate parameters comparison, the fast-switching valve SX12-JJ was selected. Based on the specification of SX12-JJ, the response time and flow rate are shown in Figure 4. To simplify the calculation process, the flow opening area of the on/off valve was linearized. From Figure 4, the opening time is about 1 ms and the closing time is about 0.5 ms.

The opening time and closing time are variable in the different external loads. The valve force diagram is shown in Figure 5. Newton's second law allows taking the balance of the forces influencing the movement of the valve:

$$F_a - F_b - F_{sp} - b_m \dot{y} - F_{cy} = M \ddot{y} \quad (24)$$

where

$$F_a = p_a \frac{\pi D_a^2}{4} \quad (25)$$

$$F_b = p_b \frac{\pi(D_a^2 - D_b^2)}{4} \tag{26}$$

$$F_{sp} = k_{sp}(y_{sp0} + y) \tag{27}$$

$$F_{cy} = p_{cy} \frac{\pi D_e^2}{4} \tag{28}$$

where p_a and p_b are the air pressure in the chamber a and chamber b , D_a and D_b are diameters of piston and piston rod, k_{sp} is the stiffness of the spring, y_{sp0} is the pre-compression length, D_e is the diameter of the valve head, M is the mass of moving parts including piston, piston rod, connector, valve, b_m is the piston viscosity coefficient. The computational procedure for air pressure in chamber a and chamber b is similar to the calculation process of cylinder pressure.

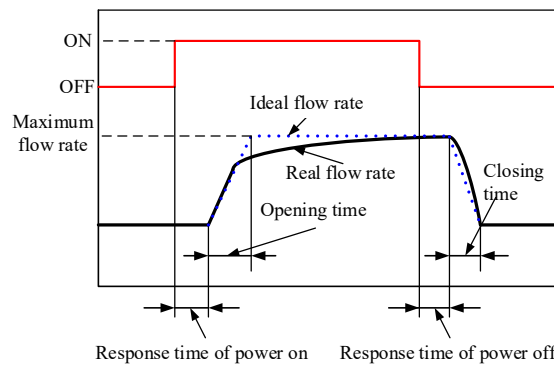


Figure 4. The response time and flow rate of SX12-JJ.

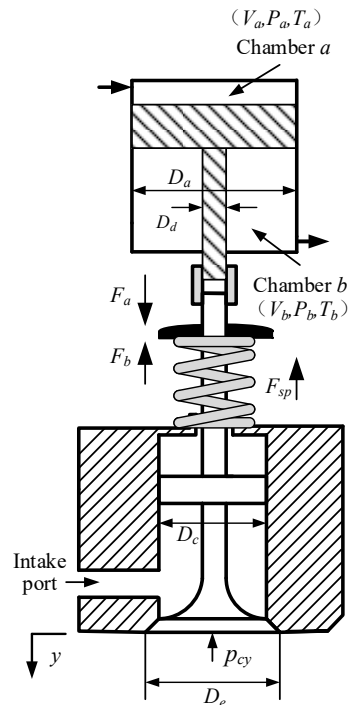


Figure 5. The diagram of valve force.

The initial parameters are shown in Table 2.

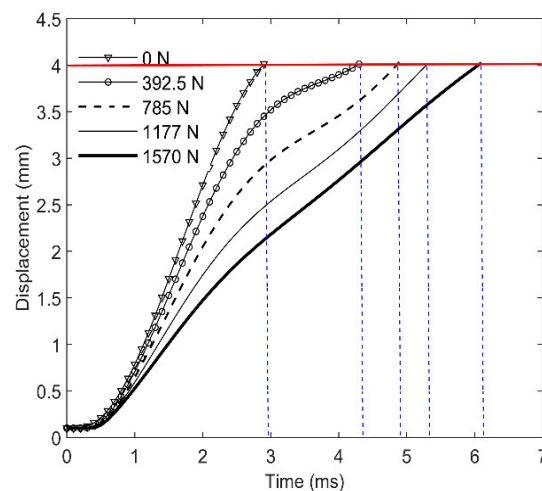
Table 2. Initial structure parameters.

Parameter	Symbol	Value
Diameter of the valve head (mm)	D_e	20
Diameter of the piston (mm)	D_a	80
Diameter of the piston rod (mm)	D_b	40
stiffness of spring (N/m)	k_{sp}	200
Diameter of force balance block (mm)	D_c	16
Stroke of cylinder (mm)	L	4
Ambient pressure (bar)	p_{atm}	1
Air pressure in the intake port (bar)	p_s	50
Air pressure supply to flow into actuator (bar)	p_p	8
Pre-compression length (mm)	y_{sp0}	1
Mass of moving parts (kg)	M	0.5
piston viscosity coefficient (N·s/m)	b_m	80

The maximum force acting on the valve can be calculated by:

$$F_{\max} = p_s \times \frac{\pi}{4} D_e^2 = 50 \times 10^5 \times \frac{3.14}{4} \times 20 \times 20 \times 10^{-6} = 1570N \quad (29)$$

When the engine opens, the pressure in the engine cylinder has not immediately reached maximum pressure. Thus, the external force was assumed to be 0 N, 392.5 N, 785 N, 1177.5 N, and 1570 N. Based on these external forces, the movement characteristics of the intake engine valve are shown in Figure 6.

**Figure 6.** Movement characteristics of the intake engine valve.

It is evident that the time corresponding to the valve to maximum lift increases when the external force increases from 0 N to 1570 N. When the external force is equal to 0 N, the time corresponding is equal to 2.9 ms; when the external force is equal to 1570 N, the time corresponding is equal to 6.1 ms. In the actual process, the external force varies with air pressure in cylinder, and the air pressure in the cylinder is lower than the supply air pressure in the intake port, owing to the throttling effect. Under normal conditions, it is easier to close the engine valve than to open it based on valve force. As described in Section 4, t_{il} , $t_{ic} - t_{id}$, $t_{ed} - t_{el}$, and $t_{ec} - t_{ed}$ should reduce as much as possible. In this paper, t_{il} , $t_{ic} - t_{id}$, $t_{ed} - t_{el}$, and $t_{ec} - t_{ed}$ are set to 5 ms.

3.2. Boundary Conditions

The system was simulated in the Matlab/Simulink software using the developed mathematical model for the preliminary investigation of the expander performance under

different valve trajectories. The simulation was initially run using arbitrary values for the model parameters. Some of the model parameters that are design dependents, such as valve actuator moving mass (m) and friction (F_{fr}), are presumed to be known values in the simulation. Table 3 shows the final values selected for the system parameters. According to the mathematical model above, each parameter can be changed for comparison while all other parameters are kept constant.

Table 3. Basic structure parameters.

Parameter	Symbol	Value
Cylinder bore (mm)	D_{cy}	85
Cylinder stroke (mm)	S_{cy}	88
Radius of the crankshaft (mm)	r	44
Ratio of crankshaft and link rod	λ	0.3
Expander cylinder clearance (mm)	x_0	4
Supply pressure (bar)	p_s	50
Number of the intake valve and exhaust valve	N_v	1
Diameter of valve small head (mm)	D_s	12
Maximum lift of intake valve (mm)	l_{imax}	4
Maximum lift of exhaust valve (mm)	l_{emax}	5
Specific heat at constant pressure (J/(kg·K))	C_p	1005
Specific heat at constant volume (J/(kg·K))	C_v	718
Gas constant (J/(kg·K))	R	287

The intake valve and exhaust valve trajectories depend on l_{iv} , t_{il} , t_{id} , t_{ic} , l_{ev} , t_{el} , t_{ed} , and t_{ec} . The pneumatic actuators are used to drive the intake valve and exhaust valve. In this paper, T_0 is set as 5 ms, which is explained in Section 3.1. Thus, $t_{id} - t_{il}$, defined as intake valve duration time can be regulated according to different rotation speeds. The exhaust valve keeps opening during the exhaust process to reduce exhaust resistance.

3.3. Intake Valve Duration Angle Optimization

This section optimizes the intake valve duration angle according to different rotation speeds. The average output power and energy efficiency are the optimization objectives shown in Equations (14) and (15). Figure 7 shows the average output power and energy efficiency obtained in different intake valve duration angles based on given conditions shown in Table 3 when the rotation speed is equal to 800 rpm.

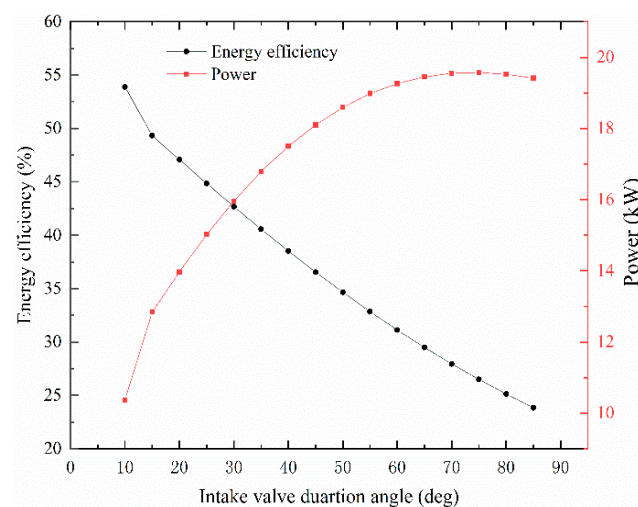


Figure 7. Average energy efficiency and output power in different intake valve duration angles.

Under most conditions, the PTE system has an inherent tradeoff between energy efficiency and output power. As shown in Figure 7, the energy efficiency decreases as the

intake valve duration angle increases. The energy efficiency reaches a maximum value when the intake valve duration angle is equal to 10° . Compared with the 85° intake valve duration angle, the energy efficiency increases by 30.05%. Initially, the output power ascends sharply with the increasing intake valve duration angle, but the amplitude of power growth decreases. Additionally, the output power peaks at approximately 19.57 kW. After this peak, the output power starts to descend slowly.

The primary reason is that the residual pressure increases with the intake valve duration angle, as shown in Figure 8.

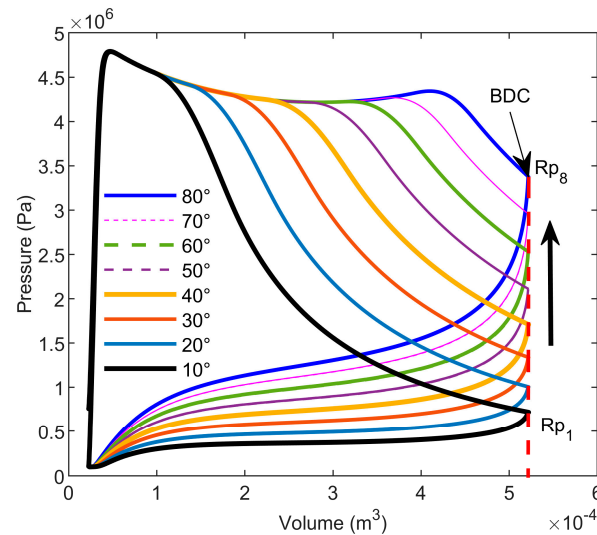


Figure 8. Pressure in expander cylinder vs. volume in different intake valve duration angle.

The primary reason is that the residual pressure increases with the intake valve duration angle, as shown in Figure 8. When the intake valve duration angle is equal to 10° , the residual pressure (RP) value is equal to about 7 bar, which is the air pressure in the expander cylinder when the piston reaches BDC. The residual pressure increases from 7 bar to 33.4 bar when the intake valve duration angle varies from 10° to 80° . The higher residual pressure leads to more energy loss. However, the output power increases with the pressure in the expander cylinder increasing. However, with the residual pressure reaching a specific value, more energy from pressurized air will be consumed during the exhaust process. Thus, the output power has an extreme value at an exact rotational speed.

Figure 9 shows an intake valve position, velocity trace, and the corresponding valve event performance parameters when the intake valve duration angle is equal to 10° .

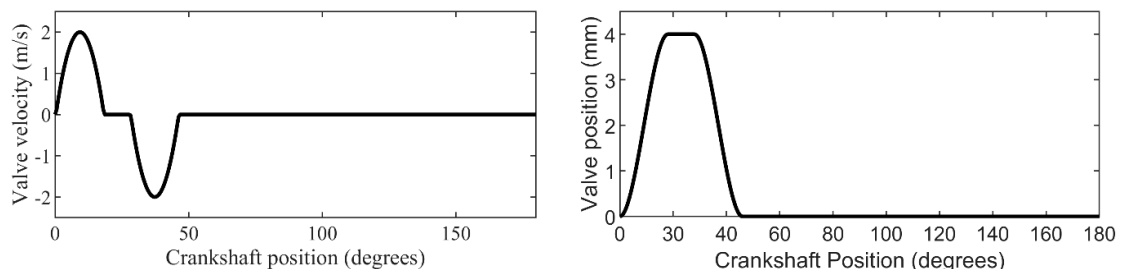


Figure 9. Intake valve position and velocity.

The expander's energy efficiency and output power cannot reach optimum at the same time. An effective, comprehensive evaluation method should be proposed to obtain the optimum intake valve duration angle based on energy efficiency and output power. This paper uses the gray relation analysis (GRA) method [15,20] to obtain the expected indicator.

The evaluation set $E = (P, \eta) = (E_1, E_2)$ is formed by the indicators in Equations (14) and (15). The calculative process of the GRA method is shown as follows:

Step 1. Calculate the decision matrix D . D_{ij} is the calculated value of E_j through the simulation model's running with different intake valve duration angles. Then, $D = (D_{ij})_{N \times 2}$ is called the gray relational decision matrix. i is No. i intake valve duration angle, and j is the indicator number.

Step 2. According to the decision matrix D , the maximum and minimum values corresponding to evaluated indicators can be obtained, expressed as $D_{min} = (D_{0min}, D_{1min})$ and $D_{max} = (D_{0max}, D_{1max})$.

Step 3. Normalization of the decision matrix. The decision matrix can be normalized by using the D_{min} and D_{max} , described by the following equation:

$$f_{ij} = \frac{D_{ij} - D_{ojmin}}{D_{ojmax} - D_{ojmin}} \quad (30)$$

Step 4. Calculated the relation degree. The relational degree between the calculated indicators and the leading indicators can be calculated by:

$$R_i = \sum_{j=1}^2 f_{ij} W_j, \quad i = 1, 2, \dots, N \quad (31)$$

where W_j is the vector of weight, $W_j = (0.6, 0.4)^T$.

The value of R_i can determine the optimal intake valve duration angle. The bigger R_i is, the more the calculated indicators fit with the leading indicators.

The optimal performance indicators and corresponding intake valve duration angles are obtained by simulating calculations in Table 4.

Table 4. Performance indicators and optimum intake valve duration angle.

Optimum Intake Valve Duration Angle (deg)	Output Power (kW)	Energy Efficiency (%)	Speed (rpm)
15	8.91	56.8	600
20	12.1	50.9	700
25	15.02	44.86	800
30	17.27	38.9	900
30	18.06	35.1	1000
30	18.23	31.2	1100

In different rotational speed conditions, optimal trajectories of the intake valve can be obtained, which are shown in Figure 10.

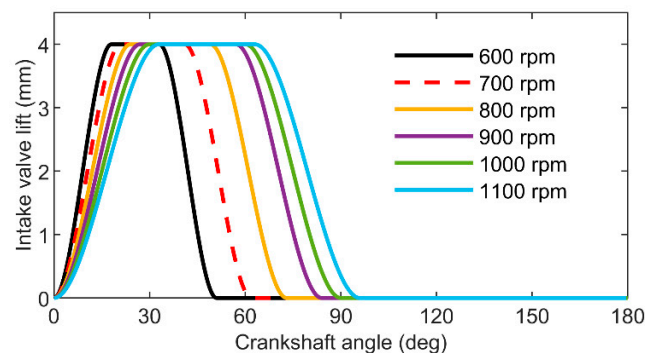


Figure 10. Optimum intake valve lift curves in different rotational speeds.

When the rotational speed is lower than 900 rpm, the intake valve duration angle is equal to 30°. When the rotation speed is higher than 900 rpm, the intake valve duration

angle is equal to 30° . Due to the different rotational speeds, the opening and closing angles of the intake valve are different during the same opening and closing times. Figure 10 gives the reference intake valve trajectories at different rotational speeds, which is the basement to control the intake valve actuator.

4. Conclusions

In this paper, an EPVVA system was proposed for independent control distributing valve parameters. Based on the EPVVA system, the working principle was introduced, and the mathematical model of the system was developed. Meanwhile, the working characteristics were obtained by numerical analysis. Trajectory planning for the intake valve and the effect of intake valve duration angle were carried out. The optimum intake valve duration angles at different rotational speeds were obtained by using the GRA method. Some conclusions can be drawn:

- (1) The energy efficiency decreases with the intake valve duration angle increasing.
- (2) Initially, the output power ascends sharply with increasing intake valve duration angle, but the amplitude of power growth decreases. When the rotational speed is equal to 800 rpm, the output power peaks at approximately 19.57 kW when the intake valve duration angle is equal to 75° , after this peak, the output power starts to descend slowly.
- (3) When the rotational speed varies from 600 rpm to 900 rpm, the corresponding intake valve duration angle increases from 15° to 30° . When the rotation speed is higher than 900 rpm, the intake valve duration angle is equal to 30° .

The future work will focus on the precise control of this VVA system and the experimental study in the actual PTE to comprehensively study the performance of the proposed system.

Author Contributions: Conceptualization, Q.Y. and Y.S.; methodology, Y.S.; formal analysis, G.S. and X.L.; investigation, G.S. and X.L.; writing—original draft preparation, Y.S.; writing—review and editing, Q.Y.; funding acquisition, Q.Y. All authors have read and agreed to the published version of the manuscript.

Funding: This research was funded by National Natural Science Foundation of China, grant number 52065054 and The APC was funded by National Natural Science Foundation of China.

Data Availability Statement: Not applicable.

Acknowledgments: The research work presented in this paper is supported by a Grant (2022LHMS05023) from the Natural Science Foundation of Inner Mongolia, the Fundamental Research Funds for Inner Mongolia University of Science and Technology, and the Beijing Outstanding Young Scientists Program (BJJWZYJH01201910006021).

Conflicts of Interest: The authors declare no conflict of interest or personal relationships that could have appeared to influence the work reported in this paper.

References

1. IEA. An Energy Sector Roadmap to Carbon Neutrality in China. 2021. Available online: <https://www.iea.org/reports/an-energy-sector-roadmap-to-carbon-neutrality-in-china> (accessed on 1 October 2022).
2. Succar, S.; Denkenberger, D.C.; Williams, R.H. Optimization of specific rating for wind turbine arrays coupled to compressed air energy storage. *Appl. Energy* **2012**, *96*, 222–234. [CrossRef]
3. Venkataramani, G.; Parankusam, P.; Ramalingam, V.; Wang, J. A review on compressed air energy storage—A pathway for smart grid and polygeneration. *Renew. Sustain. Energy Rev.* **2016**, *62*, 895–907. [CrossRef]
4. Barbour, E.R.; Pottie, D.L.; Eames, P. Why is adiabatic compressed air energy storage yet to become a viable energy storage option? *IScience* **2021**, *24*, 102440. [CrossRef] [PubMed]
5. Minutillo, M.; Lavadera, A.L.; Jannelli, E. Assessment of design and operating parameters for a small compressed air energy storage system integrated with a standalone renewable power plant. *J. Energy Storage* **2015**, *4*, 135–144. [CrossRef]
6. Li, S.; Dai, Y. Design and simulation analysis of a small-scale compressed air energy storage system directly driven by vertical axis wind turbine for isolated areas. *J. Energy Eng.* **2015**, *141*, 04014032. [CrossRef]

7. Farzaneh-Gord, M.; Izadi, S.; Pishbin, S.I.; Sheikhani, H.; Deymi-Dashtebayaz, M. Thermodynamic analysis of medium pressure reciprocating natural gas expansion engines. *Pol. J. Chem. Technol.* **2015**, *17*, 119–125. [[CrossRef](#)]
8. Liu, J.-L.; Wang, J.-H. Thermodynamic analysis of a novel tri-generation system based on compressed air energy storage and pneumatic motor. *Energy* **2015**, *91*, 420–429. [[CrossRef](#)]
9. He, W.; Wang, J. Optimal selection of air expansion machine in Compressed air energy storage: A review. *Renew. Sustain. Energy Rev.* **2018**, *87*, 77–95. [[CrossRef](#)]
10. Dumont, O.; Parthoens, A.; Dickers, R.; Lemort, V. Experimental investigation and optimal performance assessment of four volumetric expanders (scroll, screw piston and roots) tested in a small-scale organic Rankine cycle system. *Energy* **2018**, *165 Pt A*, 1119–1127. [[CrossRef](#)]
11. Hou, X.; Zhang, H.; Xu, Y.; Yu, F.; Zhao, T.; Tian, Y.; Yang, Y.; Zhao, R. External load resistance effect on the free piston expander-linear generator for organic Rankine cycle waste heat recovery system. *Appl. Energy* **2018**, *212*, 1252–1261. [[CrossRef](#)]
12. Liu, H.; Chen, Y.; Tao, G.L.; Liu, H.; Chen, Y.; Tao, G.; Jia, G.; Ding, W. Research on the displacement and stroke-bore ratio of the air-powered engine. In Proceedings of the Sixth International Conference on Fluid Power Transmission and Control, Huanggang, China, 5–8 April 2005; pp. 381–384.
13. Chen, Y.; Liu, H.; Tao, G.L. Simulation on the port timing of an air-powered engine. *Int. J. Vehicle Des.* **2005**, *38*, 259–273. [[CrossRef](#)]
14. Liu, L.; Yu, X.-L. Optimal design of ideal cycle in air powered engine. *J. Zhejiang Univ. (Eng. Sci.)* **2006**, *40*, 1815–1818.
15. Xu, Q.Y.; Shi, Y.; Yu, Q.H.; Cai, M. Virtual prototype modeling and performance analysis of the air-powered engine. *Proc. Int. Mech. Eng. C-J. Mech.* **2014**, *228*, 2642–2651.
16. Yu, Q.; Hao, X.; Tan, X. Comparative study on air distribution system for piston-type compressed air engine. *Adv. Mech. Eng.* **2017**, *9*, 1–11. [[CrossRef](#)]
17. Yu, Q.; Shi, Y.; Cai, M.; Xu, W. Fuzzy logic speed control for the engine of an air-powered vehicle. *Adv. Mech. Eng.* **2016**, *8*, 1–11. [[CrossRef](#)]
18. Shi, Y.; Xu, S.; Sun, Z.; Nie, Y.; Wang, Y. Research on the Pressure Regulator Effect on a Pneumatic Vibration Isolation System. *Chin. J. Mech. Eng.* **2022**, *35*, 128. [[CrossRef](#)]
19. Shi, Y.; Chang, J.; Wang, Y.; Zhao, X. Gas Leakage Detection and Pressure Difference Identification by Asymmetric Differential Pressure Method. *Chin. J. Mech. Eng.* **2022**, *35*, 44. [[CrossRef](#)]
20. Yu, Q.H.; Cai, M.L.; Shi, Y.; Xu, Q.Y. Optimization study on a single-cylinder compressed air engine. *Chin. J. Mech. Eng.* **2015**, *28*, 1285–1292. [[CrossRef](#)]

Disclaimer/Publisher’s Note: The statements, opinions and data contained in all publications are solely those of the individual author(s) and contributor(s) and not of MDPI and/or the editor(s). MDPI and/or the editor(s) disclaim responsibility for any injury to people or property resulting from any ideas, methods, instructions or products referred to in the content.